PAPER • **OPEN ACCESS**

A novel design of a hybrid glulam-steel substructure for the IEA 15-MW floating wind turbine

To cite this article: H H Yousef *et al* 2023 *IOP Conf. Ser.: Mater. Sci. Eng.* **1294** 012004

A novel design of a hybrid glulam-steel substructure for the IEA 15-MW floating wind turbine

H H Yousef, Y Ma*, K S Patel, and Y Xing

Faculty of Science and Technology, University of Stavanger, Norway

* Correspondence: yucong.ma@uis.no

Abstract. Wind energy has become increasingly recognised as a very promising type of renewable energy. In addition, floating offshore wind turbines have facilitated the development of electricity production in intermediate (45-150 m) and deep sea (>150 m) depths. Despite this, wind turbine manufacturing, installation, and operation may generate substantial greenhouse gas emissions. A novel hybrid glulam-steel floating substructure design is presented in this research, intended for the IEA 15 MW floating wind turbine. The objective is to contribute to advancing floating wind energy while minimising costs and carbon dioxide emissions. The objective of the novel design is to substitute steel with glued laminated lumber (glulam). It showcases an altered iteration of the UMaine VolturnUS-S semi-submersible platform originally created for the IEA 15 MW turbine. Before selecting one of three preliminary hybrid wood-steel models, the Ansys Workbench 2020 R1 is used to evaluate and appraise them per a set of criteria extracted from pertinent timber and steel standards. The chosen hybrid design conserves about 590 metric tonnes of steel mass compared to the UMaine VolturnUS-S semi-submersible platform. The selected model is then validated by executing a fully coupled aero-hydro-servo-elastic dynamic analysis with OpenFAST. Consideration is limited to the ultimate limit state design (ULS) for normal and severe operating situations. The utilisation factor of the glulam supporting structure for the IEA 15 MW turbine ranges from 74% to 94%, indicating that it is an effective load-bearing solution.

1. Introduction

The achievement of the net-zero emission objective by 2050 might be facilitated by the development of wind turbines with less CO_2 footprint [1]. The majority of offshore wind turbines are currently bottom-fixed monopile turbines. However, 80% of offshore wind potential is situated at depths beyond 60 m, where bottom fixed wind turbines are not cost-effective [2]. In contrast, floating offshore wind turbines (FOWTs) provide a significant benefit in such deep seas. As the International Electrotechnical Commission (IEC) [3] specified, floating wind turbines are designed to endure harsh offshore environmental conditions for at least two decades. Expanding offshore wind farms, particularly using floating wind turbines in connection with the global transition to renewable energy sources, requires more research and development in engineering, procurement, maintenance, and CO_2 emissions.

The findings of [4] indicate that the materials used in the construction and maintenance of a 6 MW spar buoy wind turbine and a 6 MW raft-buoy wind turbine have a substantial impact on the Carbon Intensity of Electricity (CIE), which varies between 26.1 and 78.7 CO_{2eq}/kWh. The aforementioned research underscores the need to develop novel technologies that reduce the overall steel mass to

minimise the turbine's CO_2 footprint since steel production usually generates significant amounts of CO_2.

The strong, corrosion-resistant, stable, and environmentally friendly glued laminated wood (glulam) is superior to steel in many ways, including cost, strength-to-weight ratio, and prefabrication possibilities. With centuries of experience in the construction industry, we now have a greater understanding of efficient joint selection, constraints, and glulam construction procedures [5]. The glulam-only Mjørstårnet 18-story structure, which was finished in 2019, is the tallest wooden structure in the world [6]. In Bjorko, Sweden, Modvion constructed a 30-meter-tall timber tower in 2020 [7]. Stora Enso, a biomaterials and wood construction company, and Voodin Blade Technology GmbH, a German business specialising in the production of rotor blades for wind turbines, have just initiated a collaborative effort to substitute heavier, non-renewable wind turbine blades with wooden ones.

This study aims to propose a novel hybrid glulam-steel substructure design for the semi-submersible IEA 15 MW wind turbine (refer to Figure 1). The IEA 15 MW was chosen as the reference wind turbine because it corresponds to the currently largest state-of-the-art wind turbines in the market [8]. Three distinct hybrid models are initially constructed and evaluated using the ANSYS Workbench 2020 R1. Then, these three models were compared to identify the optimal one that maximises material mass while maintaining acceptable utilisation factors. A fully coupled aero-hydro-servo-elastic dynamic study is then conducted with OpenFAST to verify the identified optimal model. The design investigation is limited to the ultimate limit state (ULS) design of the turbine, which includes both severe and ordinary operating conditions.

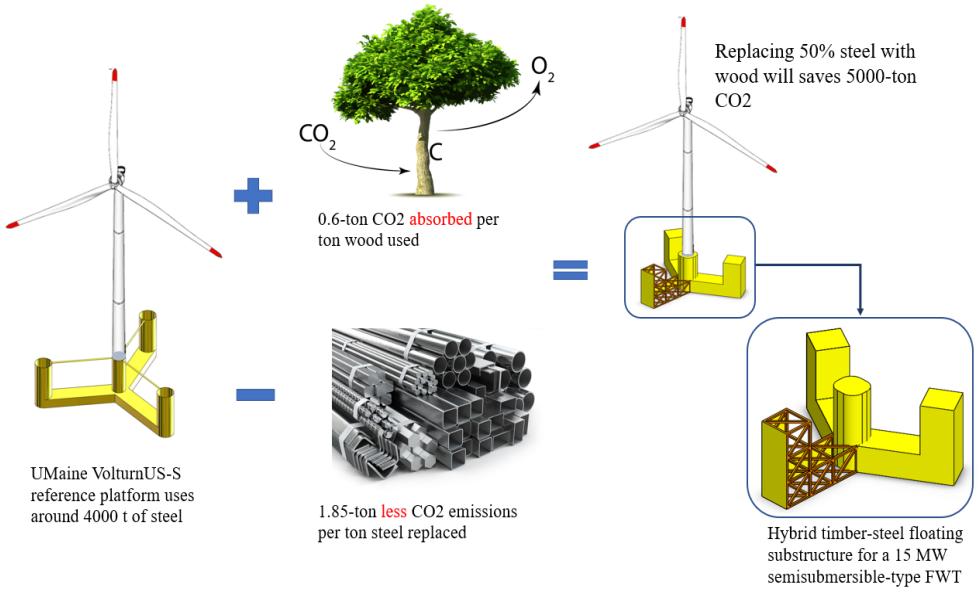

Figure 1. The environmental impact of using wood as a replacement for steel

2. System Description

This study employs the IEA 15-MW floating wind turbine (FWT) [9]. The FWT system will be described in the following sections in two parts. Following a description of the reference wind turbine, the characteristics of the first UMaine VolturnUS-S semi-submersible platform and the mooring system will be discussed.

2.1. IEA Wind 15-Megawatt reference FWT

The reference wind turbine (RWT) utilised in this study has a capacity of 15 MW. It was constructed following the International Electrotechnical Commission's (IEC) Class 1B wind regime and consists of three blades rotating clockwise upwind. Additionally, it is outfitted with a collective pitch and variable speed control system. Table 1 provides an overview of the IEA Wind 15-MW RWT.

Table 1. General parameters of IEA Wind 15-MW RWT [8,9]

Parameter	Value	Unit
Power rating	15	MW
Rotor orientation, configuration	Upwind, 3 blades	-
Control	Variable speed, collective pitch	-
Drivetrain	Low-speed, direct drive	
Cut-in, rated, cut-out wind speed	3, 10.59, 25	m/s
Rotor, hub diameter	240, 7.94	m
Hub height	150	m
Design tip-speed ratio	9	-
Minimum rotor speed	5	rpm
Maximum rotor speed	7.56	rpm
Maximum tip speed	95	m/s
Water depth	200	m
Total system mass	20,093	t
Platform mass	17,839	t
Rotor nacelle assembly mass	991	t
Tower mass	1,263	t
Tower base diameter	10	m

2.2. UMaine VolturnUS-S reference semi-submersible platform

The UMaine VolturnUS-S semi-submersible floating sub-structure design will serve as the basis for the novel hybrid design proposed in this study. The floater has three outer columns arranged in a circle, with a fourth column in the centre. A star-shaped pontoon with a triangular cross-section at its apex supports the columns. Three radial struts with a diameter of 0.9 metres are used to connect the columns at the uppermost point. The floater's location is maintained by the use of three catenary mooring lines (refer to Figure 2 (b)). Table 2 provides further information on the UMaine VolturnUS-S semi-floater, while Table 3 describes the mooring system in greater detail.

Table 2. Semi-submersible Platform Properties [9]

Parameter	Value	Unit
Hull displacement	20,206	m^3
Hull steel mass	3,914	t
Tower interface mass	100	t
Ballast mass (fixed/fluid)	2,540/11,300	t
Draft	20	m
Freeboard	15	m
Vertical center of gravity from SWL	-14.94	m
Vertical center of buoyancy from SWL	-13.63	m
Roll inertia about the center of gravity	1.251×10^{10}	$kg\cdot m^2$
Pitch inertia about the center of gravity	1.251×10^{10}	$kg\cdot m^2$
Yaw inertia about the center of gravity	2.367×10^{10}	$kg\cdot m^2$

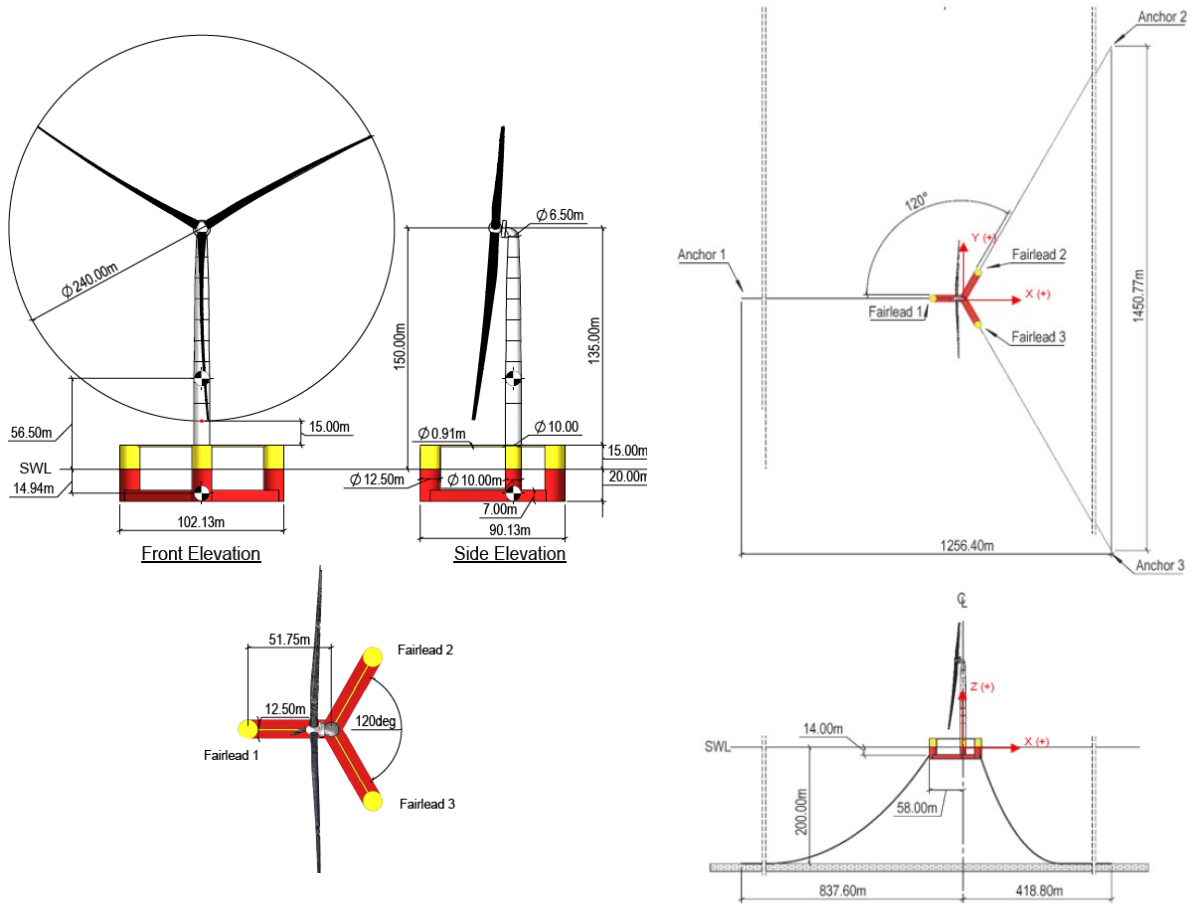

(a) (b)

Figure 2. (a) Main dimensions of the UMaine VolturnUS-S floater of the 15-MW wind turbine; (b) Sketch of the mooring system in the 15-MW FWT

Table 3. Mooring system's properties [9]

Parameter	Value	Unit
System type & number of lines	Chain Catenary & 3 Lines	-
Line type	Studless R3 Chain	-
Line breaking strength	22.286	kN
Fairlead depth	14	m
Dry line linear density	685	kg/m
Extensional stiffness	3270	MN
Line unstretched length	850	m
Fairlead pretension	2,437	kN
Fairlead angle from SWL	56.4	deg

3. Finite Element Analysis of Three Concept Configurations

As indicated in Figure 3, three configurations are recommended for this study. Figure 3 depicts the configuration of the glulam supporting system for a single pontoon and the middle region connecting all three pontoons. The outside dimensions of each configuration are similar to those of the UMaine platform. 0.05 m steel plates are used as the hull plates that are in contact with the water and are attached

to the outer of the glulam structures. No glulam structures will be in contact with the water. Additional information about the design details may be found in Appendix A [10] of Yousef (2023).

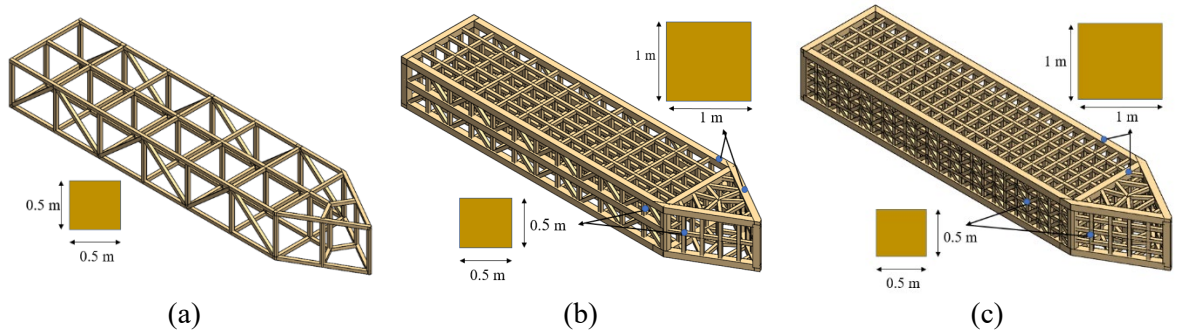

Figure 3. Glulam-based supporting structures for the three proposed configurations

3.1. Load and boundary conditions

To simplify the design procedure, only the maximum aerodynamic load is taken into account at the specified rated wind velocity, together with the corresponding hydrostatic pressure. Further details on loads and boundary conditions are available in [10].

3.2. Material properties

Table 4 presents the material properties used.

Table 4. Material properties of the plate's steel and glulam Gl30h assigned for the beams [11]

Property	Glulam G30h for beams	Steel for plates	Unit
Density	480	7850	kg/m^3
Young's Modulus X(L) direction	1.36×10^{10}		Pa
Young's Modulus Y(R) direction	3×10^{8}	2×10^{11}	Pa
Young's Modulus Z(T) direction	3×10^{8}		Pa
Poisson's Ratio XY	0.21		-
Poisson's Ratio YZ	0.21	0.3	-
Poisson's Ratio XZ	0.24		-
Shear Modulus XY	6.5×10^{8}		Pa
Shear Modulus YZ	6.5×10^{8}	7.692×10^{11}	Pa
Shear Modulus XZ	6.5×10^{8}		Pa
Tensile Yield Strength	2.4×10^{7}	2.5×10^{8}	Pa
Compressive Yield Strength	3×10^{8}	2.5×10^{8}	Pa

3.3. Mesh element type

Quadrilateral element types and more details on the element type are provided in Table 5.

Table 5. Element type details

Part	Element name IDs	Element shape
Plates	SHELL181	QUAD4
Beams	BEAM188	BEAM3

3.4. Design criteria

The following criteria were used for the design:

- Glulam under combined bending and axial tension criteria [12]

Criteria 1
$$\frac{\sigma_{t,0,d}}{f_{t,0,d}} + \frac{\sigma_{m,y,d}}{f_{m,y,d}} + k_m.\frac{\sigma_{m,z,d}}{f_{m,z,d}} \leq 1 \quad (1)$$

Criteria 2
$$\frac{\sigma_{t,0,d}}{f_{t,0,d}} + k_m.\frac{\sigma_{m,y,d}}{f_{m,y,d}} + \frac{\sigma_{m,z,d}}{f_{m,z,d}} \leq 1 \quad (2)$$

$\sigma_{t,0,d}$ is the design tensile stress along the grain, $\sigma_{m,y,d}$ and $\sigma_{m,z,d}$ are the design bending stresses around the y and z axes, $f_{t,0,d}$ is the design tensile stress along the grain, $f_{m,y,d}$, and $f_{m,z,d}$ are the corresponding design bending strengths, and k_m is a factor that makes allowance for the re-distribution of stresses and the effect of inhomogeneities of the material, and is 0.7 for glulam with a rectangular cross-section.

- Glulam under combined bending and axial compression criteria [12]

Criteria 3
$$\left(\frac{\sigma_{c,0,d}}{f_{c,0,d}}\right)^2 + \frac{\sigma_{m,y,d}}{f_{m,y,d}} + k_m.\frac{\sigma_{m,z,d}}{f_{m,z,d}} \leq 1 \quad (3)$$

Criteria 4
$$\left(\frac{\sigma_{c,0,d}}{f_{c,0,d}}\right)^2 + k_m.\frac{\sigma_{m,y,d}}{f_{m,y,d}} + \frac{\sigma_{m,z,d}}{f_{m,z,d}} \leq 1 \quad (4)$$

where $\sigma_{c,0,d}$ is the design compressive stress along the grain, $f_{c,0,d}$ is the design's compressive strength along the grain.

- Glulam beam stability criteria [12]

Criteria 5
$$\left(\frac{\sigma_{m,d}}{k_{crit}.f_{m,d}}\right)^2 + \frac{\sigma_{c,0,d}}{k_{c,z}.f_{c,0,d}} \leq 1 \quad (5)$$

where $\sigma_{m,d}$ is the design bending stress, k_{crit} is a factor that considers the reduced bending strength due to lateral buckling, and $k_{c,z}$ is an instability factor. The values of k_{crit} and $k_{c,z}$ can be calculated based on equations given in EN 1995-1-1 standard [12].

- Steel plates yielding criteria [13]

Criteria 6
$$\gamma_m \frac{\sigma_{j,d}}{R_k} \leq 1 \quad (6)$$

$\sigma_{j,d}$ is von Mises equivalent design stress, R_k is the characteristic strength and $\gamma_m = 1.15$ taken for plated structures.

The utilisation factor for configuration (b) as per the first criterion is shown in Figure 4. A comparison of the maximum utilisation factors for each configuration, as determined by the aforementioned criteria, is presented in Table 6. The results indicate that design (b) minimises glulam mass while maintaining an acceptable utilisation factor. Consequently, further investigations are only made on design (b).

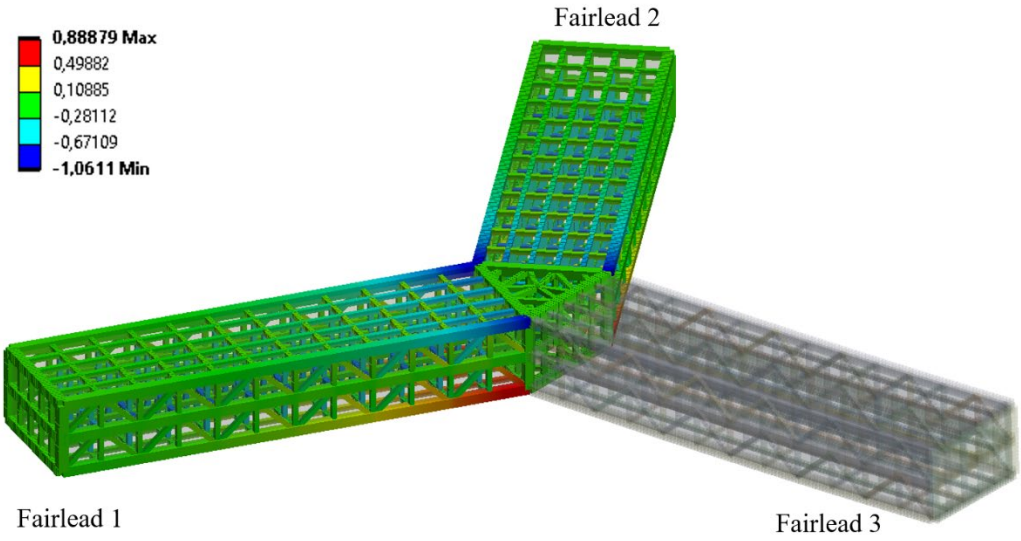

Figure 4. Utilisation factor corresponding to the 1st combined bending and tension criteria for glulam, configuration (b)

Table 6. Max utilisation factor for three hybrid configurations

Material	Design criteria	Config. (a)	Config. (b)	Config. (c)
Glulam	$UF_{max,\ 1}$	1.03	0.75	0.76
	$UF_{max,\ 2}$	1.04	0.80	0.82
	$UF_{max,\ 3}$	5.63	0.90	0.94
	$UF_{max,\ 4}$	5.36	0.90	0.94
	$UF_{max,\ 5}$	1.13	0.89	0.88
Steel	$UF_{max,\ 6}$	3.60	0.91	0.83

4. Hydro-Servo-Aero-Elastic analysis using OpenFAST

This study uses OpenFAST, an open-source modelling programme developed by the National Renewable Energy Laboratory (NREL), to analyse the 15-MW FWT in a fully coupled aero-hydro-elastic-servo dynamic manner. AeroDyn [14], HydroDyn [15], ServoDyn, ElastoDyn, TurbSim, InflowWind, and MoorDyn [16] are some of the software modules that the OpenFAST code integrates to simulate mooring system dynamics, control dynamics, hydrodynamic loads on rotor blades, and hydrodynamic loads on floaters.

Yousef [10] states that the hybrid floater exhibits the same CoB, CoG, mass, and moments of inertia as the UMaine VolturnUS-S platform, except for a substantial reduction in the mass of the steel and concrete components. Furthermore, the hybrid floater's outward dimensions and shape are also similiar to those of the UMaine VolturnUS-S platform. The aforementioned conditions provide automatic fulfilment of the stability and eigenfrequency criteria. Furthermore, the hydrodynamic characteristics pre-established for the UMaine VolturnUS-S platform [9] may be used immediately in the hydrodynamic analysis of the hybrid floater configuration (b).

Design load cases (DLC)

In order to assess the performance of the hybrid floater, a subset of IEC design load instances pertaining to the East Coast of the United States is used [17, 18]. See Table 7. All simulations were executed for 720 seconds under the assumption that the wind and waves are aligned at an angle of 0 degrees.

Table 7. IEC Design load cases

	DLC number	Wind condition	U_{hub} (m/s)	H_s (m)	T_p (sec)	Gamma shape factor
1.1	1	NTM	4.00	1.10	8.52	1.00
	2		24.00	4.52	9.45	1.89
1.3	3	ETM	4.00	1.10	8.52	1.00
	4		24.00	4.52	9.45	1.89
1.6	5	NTM	4.00	6.30	11.50	2.75
	6		24.00	9.80	14.10	2.75

where ETM is the Extreme turbulence model and NTM is the Normal turbulence model.

Using OpenFAST, all the total time-varying loads on the tower base and mooring line tension, such as TwrBsFxt, TwrBsFyt, TwrBsFzt, TwrBsMxt, TwrBsMyt, TwrBsMzt, FAIRTEN1, FAIRTEN2 are obtained.

5. Local Analysis

5.1. FEA Model

The loads obtained from OpenFAST are used to re-analyse model (b) (see Figure 5).

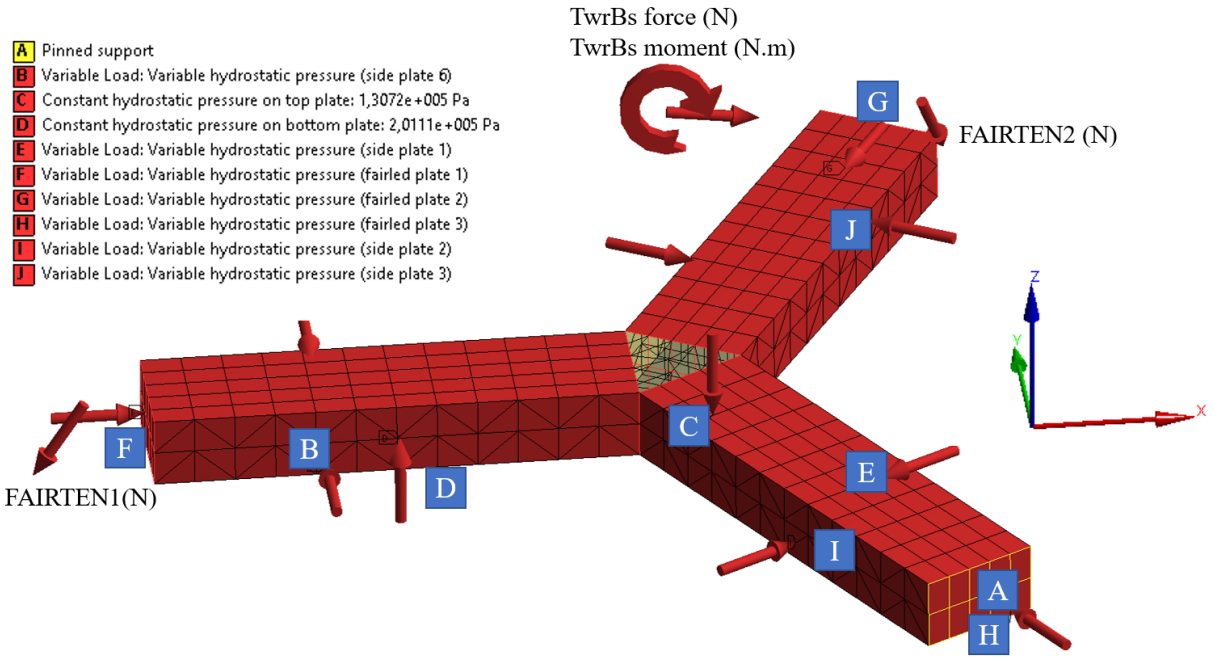

Figure 5. Actual loads acting on the hybrid design, configuration (b) (ANSYS)

5.2. Response Surface Methodology (RSM)

Utilising mathematical regression, response surface methodology (RSM) is a statistical technique that may be used to establish the relationships between several inputs and one or more outputs. Using a response surface minimises computing time by eliminating the need to execute thousands of simulations that account for various load combinations (obtained at each time step Δt over the simulation duration).

5.2.1. Design of experiment (DoE)

There are several methods for generating experimental design points in ANSYS Workbench, including the Box-Behnken design, central composite design, and optimum space-filling design, among others. In this study, the core composite design is used. 285 design points are generated in accordance with the higher and lower limits specified in Table 8.

Table 8. Upper and lower bounds assigned for input load variables

	TwrBsFxt	TwrBsFyt	TwrBsFzt	TwrBsMxt
Lower bound	-3×10^6	-2×10^6	-3×10^7	-8×10^7
Upper bound	9×10^6	2×10^6	3×10^7	2×10^8
	TwrBsMyt	TwrBsMzt	FAIRTEN1	FAIRTEN2
Lower bound	-4×10^8	-4×10^7	1×10^6	1×10^6
Upper bound	7×10^8	4×10^7	6×10^6	3×10^6

5.2.2. Construction of response surface

The response surface may be constructed using ANSYS Workbench in various methods, such as Kriging, traditional second-order regression, non-parametric regression, and more. This study generates the response surface by generic aggregation, which employs a genetic algorithm to solve several response surfaces concurrently while taking into account the response surface's correctness and stability at the design stage. The mathematical formulation of the generic aggregation strategy is given in Equation (7).

$$\hat{y}_{ens}(x) = \sum_{i=1}^{N_m} w_i \,.\, \hat{y}_i(x) \tag{7}$$

where $\hat{y}_{ens}$ is the ensemble prediction, N_m is the total number of metamodels used and $\hat{y}_i$, w_i are the prediction and weight factor of the $i-th$ response surface.

The results derived from the ANSYS workbench's goodness of fit option indicate that the response surface produced satisfies the investigated model well (refer to Table 9).

Table 9. Goodness of fit results

	$\mathrm{UF}_{max,\ 1}$	$\mathrm{UF}_{max,\ 2}$	$\mathrm{UF}_{max,\ 3}$	$\mathrm{UF}_{max,\ 4}$	$\mathrm{UF}_{max,\ 5}$	$\mathrm{UF}_{max,\ 6}$
Coefficient of Determination (best value=1)						
Learning Points	1	0.999	0.999	1	0.999	1
Cross-Validation on Learning Points	0.979	0.990	0.946	0.907	0.957	0.948
Maximum Relative Residual (best value=0%)						
Learning Points	0	0.208	0.055	0	0.183	0
Verification Points	3.221	1.755	7.290	6.449	3.183	1.564

Cross-Validation on Learning Points	2.726	2.185	7.172	8.251	4.040	1.818
Root Mean Square Error (best value=0)						
Learning Points	0	0	0	0	0	0
Verification Points	0.017	0.009	0.027	0.032	0.014	0.006
Cross-Validation on Learning Points	0.003	0.003	0.009	0.01	0.005	0.002
Relative Root Mean Square Error (best value=0%)						
Learning Points	0	0.048	0.04	0	0.059	0
Verification Points	2.164	1.188	3.907	4.253	1.667	0.797
Cross-Validation on Learning Points	0.397	0.41	1.122	1.201	0.517	0.239

5.3. Parameter correlation study

To minimise the overall processing time, the correlation analysis seeks to identify the inputs that have the most significant impact on the output of interest. This allows for identifying worst-case load combinations with fewer inputs taken into account at their maximum and lowest levels.

The correlation coefficients between the load input factors and the output stress variables vary substantially following the direction of each individual load, according to the findings of the correlation research [10]. Nevertheless, the research emphasised that some inputs—TwrBsFxt, TwrBsFzt, TwrBsMyt, FAIRTEN1, FAIRTEN1, and FAIRTEN2—have a substantial impact on the resultant output and should be taken into account when determining the worst-case load combinations [10].

5.4. Results

Table 10 presents the highest utilisation factors for each design load situation, which are determined by the worst-case load combinations. Each combination of worst-case loads represents the most significant or most negligible value of one of the input load variables. The six utilisation factors for each of the specified load combinations are then retrieved using the response surface. The utilisation of glulam beams increases by as much as 78% when subjected to combined bending and compression and by as much as 85% when subjected to combined bending and tension. Nevertheless, the beams maintain 94% of their initial capability despite resisting buckling.

Table 10. The maximum utilisation factors expected for each of the design loads

DLC number	Wind condition	Glued laminated timber					Steel
		$UF_{max,\ 1}$	$UF_{max,\ 2}$	$UF_{max,\ 3}$	$UF_{max,\ 4}$	$UF_{max,\ 5}$	$UF_{max,\ 6}$
1	NTM	0.7679	0.8175	0.7417	0.7548	0.9085	0.8153
2		0.7908	0.8406	0.7793	0.7763	0.9339	0.8243
3	ETM	0.7776	0.8280	0.7581	0.7633	0.9196	0.8194
4		0.7914	0.8414	0.7805	0.7767	0.9349	0.8246
5	NTM	0.7834	0.8331	0.7667	0.7690	0.9253	0.8213
6		0.7943	0.8436	0.7834	0.7804	0.9372	0.8256

6. Conclusion

A novel hybrid timber-steel floating substructure for a 15 MW semi-submersible-type FWT is described in this article. An initial design study was carried out by simulating and comparing the three finite

element models using ANSYS Workbench 2020 R1. The findings indicate that configuration (b) provides satisfactory utilisation factors while maintaining a minimum glulam mass (cost). In addition, the chosen hybrid configuration reduces steel mass by about 590 metric tonnes as compared to the UMaine VolturnUS-S semi-submersible platform. The hydrodynamic data supplied for the UMaine VolturnUS-S semi-submersible platform [9] were used in the hybrid model to conduct a completely nonlinear aero-hydro-servo-elastic simulation, taking into consideration the similarity in shape, mass properties, CoG, and CoB. A re-analysis was conducted on Model (b) using the loads generated by OpenFAST. Following this, the response surface approach is used to reduce the total computation time. In order to identify the input combinations with the highest utilisation factors (outputs) under the worst-case load conditions, parameter correlation analysis was undertaken. The results of the parameter correlation analysis indicated that the resultant utilisation factors exhibited a significant and variable association with TwrBsFxt, TwrBsFzt, TwrBsMyt, FAIRTEN1, FAIRTEN2, and FAIRTEN1. The conclusive findings indicate that glulam may serve as a viable substitute for structural steel in the context of IEA 15 MW. The utilisation factor for the various criteria fluctuates between 0.74 and 0.94, including both typical and severe operating situations. The lack of variation in the utilisation factor values among the several DLCs underscores the criticality of hydrostatic pressure as a load that drives the design.

Reference

[1] IEA 2020, *World energy outlook 2020*. (OECD Publishing).
[2] WindEurope 2018, *Floating offshore wind energy-a policy blueprint for europe floating offshore wind energy*.
[3] Igba J, Alemzadeh K, Durugbo C and Henningsen K 2015, "Performance assessment of wind turbine gearboxes using in-service data: Current approaches and future trends," *Renewable Sustainable Energy Rev.,* **50**, 144-159.
[4] Pulselli R, Maccanti M, Bruno M, Sabbetta A, Neri E, Patrizi N and Bastianoni S 2023, Benchmarking Marine Energy Technologies Through LCA: Offshore Floating Wind Farms in the Mediterranean. Front, *Perspectives for marine energy in the mediterranean area volume II,* **16648714**, p 18.
[5] Porteous J and Kermani A 2013, *Structural timber design to Eurocode 5* (John Wiley & Sons).
[6] Abrahamsen R, Mjøstårnet-Construction of an 81 m tall timber building. Available at: https://www.moelven.com/globalassets/moelven-limtre/mjostarnet/mjostarnet---construction-of-an-81-m-tall-timber-building_presentation.pdf (Accessed: 20.10.2023)
[7] Modvion 2020, The first wooden wind power tower has been erected in Sweden. Available at: https://modvion.com/news/the-first-wooden-wind-power-tower-has-been-erected-in-sweden/ (accessed: 20.10.2023)
[8] Gaertner E, Rinker J, Sethuraman L, Zahle F, Anderson B, Barter G E, Abbas N J, Meng F, Bortolotti P and Skrzypinski W 2020, *IEA wind TCP task 37: definition of the IEA 15-megawatt offshore reference wind turbine*, National Renewable Energy Lab.(NREL), Golden, CO (United States).
[9] Allen C, Viscelli A, Dagher H, Goupee A, Gaertner E, Abbas N, Hall M, and Barter G 2020, *Definition of the UMaine VolturnUS-S reference platform developed for the IEA Wind 15-megawatt offshore reference wind turbine*, National Renewable Energy Lab.(NREL), Golden, CO (United States).
[10] Yousef H H 2023, *Design and analysis of a hybrid timber-steel floating substructure for a 15 MW semi-submersible-type FWT*, (Master Thesis: University of Stavanger).
[11] European Committee for Standardization CEN 2013, *NS-EN 14080: 2013 NA: 2016 Timber structures-Glued laminated timber and glued solid timber Requirements*.
[12] European Committee for Standardization CEN 2006, *Eurocode 5: Design of timber structures - Part 1-1: General -Common rules and rules for buildings*.
[13] Det Norske Veritas (DNV) 2011, *DNV-OS-C101: Design of Offshore Steel Structures General (LRFD Method)*.
[14] Moriarty P J and Hansen A C 2005, *AeroDyn Theory Manual,* NREL/TP-500-36881 (National

Renewable Energy Lab.: Golden).
[15] National Renewable Energy Laboratory (NREL) 2023. *OpenFAST Documentation*, 12.04.2023; https://openfast.readthedocs.io/en/dev/index.html.
[16] Hall M 2015, *MoorDyn user's guide*, (Department of Mechanical Engineering, University of Maine: Orono, ME, USA).
[17] Viselli A M, Goupee A J and Dagher H J 2015, Model test of a 1: 8-scale floating wind turbine offshore in the gulf of maine, *J. Offshore Mech. Arct. Eng.,* **137**, 2015.
[18] Stewart G M, Robertson A, Jonkman J, and Lackner M A 2016, The creation of a comprehensive metocean data set for offshore wind turbine simulations, *Wind Energy,* **19**, 1151-1159.